Carcinogenesis vol.21 no.5 pp.1051–1057, 2000

Cadmium mutagenicity and human nucleotide excision repair protein XPA: CD, EXAFS and $^{1}H/^{15}N$-NMR spectroscopic studies on the zinc(II)- and cadmium(II)-associated minimal DNA-binding domain (M98–F219)

Garry W.Buchko, Nancy J.Hess and Michael A.Kennedy[1]

Pacific Northwest National Laboratories, Environmental Molecular Sciences Laboratory and Biogeochemistry Resources, Richland, WA 99352, USA

[1]To whom correspondence should be addressed
Email: ma_kennedy@pnl.gov

Human XPA is a 31 kDa protein involved in nucleotide excision repair (NER), a ubiquitous, multi-enzyme pathway responsible for processing multiple types of DNA damage in the eukaryotic genome. A zinc-associated, C4-type motif (C105-X_2-C108-X_{17}-C126-X_2-C129) located in the minimal DNA-binding region (M98–F219) of XPA (XPA-MBD) is essential for damaged DNA recognition. Cadmium is a known carcinogen and can displace the zinc in many metal-binding proteins. It has been suggested that the carcinogenic properties of cadmium may result from structural changes effected in XPA when Cd^{2+} is substituted for Zn^{2+} in the metal-binding site. The solution structure of XPA-MBD containing zinc(II) has recently been determined [Buchko *et al.*, (1998) *Nucleic Acids Res.*, 26, 2779–2788; Buchko *et al.*, (1999) *Biochemistry*, 38, 15116–15128]. To assess the effects of cadmium(II) substitution on the structure of XPA-MBD, XPA-MBD was expressed in minimal medium supplemented with cadmium acetate to yield a protein that was almost exclusively (>95%) associated with cadmium(II) (CdXPA-MBD). Extended X-ray absorption fine structure spectra collected on ZnXPA-MBD and CdXPA-MBD in frozen (77 K) 15% aqueous glycerol solution show that the metal is coordinated to the sulfur atoms of four cysteine residues with an average metal–sulfur bond length of 2.34 ± 0.01 and 2.54 ± 0.01 Å, respectively. Comparison of the circular dichroism, two-dimensional $^{1}H,^{15}N$-HSQC, and three-dimensional ^{15}N-edited HSQC–NOESY spectra of ZnXPA-MBD and CdXPA-MBD show that there are no structural differences between the two proteins. The absence of major structural changes upon substituting cadmium(II) for zinc(II) in XPA suggests that cadmium-induced mutagenesis is probably not due to structural perturbations to the zinc-binding core of XPA.

Introduction

The genomic DNA of all organisms is constantly being damaged by endogeneous reactions, such as hydrolysis, oxidation and methylation, and by reactions with exogeneous agents, such as ultraviolet (UV) and ionizing radiation and environmental chemical mutagens and carcinogens. Over time, this DNA damage leads to carcinogenesis, aging and genetic diseases (1,2). The cellular response is to repair and remove the DNA damage through a number of highly conserved repair mechanisms (2). Nucleotide excision repair (NER) is a DNA repair pathway responsible for removing many structurally unrelated DNA lesions from the genome (3,4) and is especially important for protecting eukaryotic organisms from the carcinogenic effects of solar UV light.

In NER, six repair factors orchestrate the excision of damaged DNA in the form of a 24–32 bp oligomer. These six repair factors are replication protein A (RPA), XPC, TFIIH, XPG, XPF-ERCC1 and XPA (3). Both XPA and RPA are essential for lesion recognition and lesion removal by NER (5). XPA appears to play a central, multifunctional role in NER (6). In addition to preferentially binding damaged over undamaged DNA (7–9), human XPA interacts with other NER proteins including ERCC1 (10), TFIIH (11), RPA (12,13), and XPC-HR23B (14).

The DNA-binding region of XPA is located within a 122 amino acid polypeptide between M98 and F219 (15). The solution structure of XPA-MBD has been determined; it consists of two subdomains, a zinc-binding core and a loop-rich subdomain joined together by a linker sequence (16–18). Zinc-associated domains are found in many DNA-binding proteins where they often play a direct role in binding DNA (19). While cysteine replacement studies show that the zinc-containing motif in XPA is essential for NER activity (9,20) chemical shift mapping studies indicate that it does not play a direct role in binding DNA (16–18). Instead, the DNA binding surface of XPA is located in the loop-rich subdomain (16–18). Regions of the zinc-binding core, together with regions of the loop-rich subdomain, form the binding surface for the largest subunit of RPA (RPA70) (16–18).

It is possible to replace the zinc in some zinc-binding proteins with cadmium (21,22), a known carcinogen (23). *In vivo* studies show that the mutation frequency of cells exposed to UV irradiation increases in the presence of cadmium(II) (24) which may be linked to its interference with the repair of UV-induced DNA damage (25). Furthermore, gel-mobility shift assays with HeLa nuclear cell extracts show that cadmium alters the ability of two proteins, of about the same molecular weight as XPA, to bind damaged DNA (26). The chemical mechanism of cadmium mutagenicity is not known (27). One hypothesis is that cadmium displaces the zinc in DNA-binding proteins involved in NER, such as XPA, and that the resulting structural changes hinder, or prevent, the protein from binding damaged DNA or from interacting with other NER proteins (26,28). To determine if the solution structure of XPA-MBD is affected by the replacement of the Zn^{2+} with Cd^{2+}, recombinant XPA-MBD containing Cd^{2+} was expressed, purified and then characterized by circular dichroism (CD), extended X-ray absorption fine structure (EXAFS) and NMR spectroscopy.

Materials and methods

Preparation of ^{15}N-labeled ZnXPA-MBD and CdXPA-MBD

The DNA coding sequence for human XPA-MBD (M98–F219) was cloned into the vector pET-11d and transfected into the host *Escherichia coli* bacterial

Abbreviations: CD, circular dichroism; CdXPA-MBD, cadmium associated XPA-MBD; EXAFS, extended X-ray absorption fine structure; HSQC, heteronuclear single quantum coherence; NER, nucleotide excision repair; NMR, nuclear magnetic resonance; UV, ultraviolet; XPA-MBD, minimal DNA-binding domain of human NER protein XPA (M98–F219); ZnXPA-MBD, zinc associated XPA-MBD.

© Oxford University Press

strain BL21(DE3)pLysS (Novagen, Madison, WI). Uniformly ^{15}N-labeled ZnXPA-MBD was expressed and purified as described previously (16,29). The same procedure was followed to express and purify CdXPA-MBD except for the supplementation of the minimal medium to a final concentration of 0.01 mM cadmium acetate [$Cd(CH_3CO_2)_2{\cdot}2H_2O$; Sigma, St Louis, MO] instead of zinc acetate [$Zn(CH_3CO_2)_2{\cdot}2H_2O$; Sigma]. Mass determination of CdXPA-MBD by electrospray ionization mass spectral analysis of a non-labeled preparation (TSQ 7000 triple-quadrupole mass spectrometer; Finnigan, San Jose, CA) confirmed the predicted molecular weight for a protein containing a 1:1 stoichiometric ratio of cadmium and indicated that the metal in the CdXPA-MBD preparation was primarily (>95%) cadmium. The final yield of CdXPA-MBD obtained from the soluble fraction was ~30 mg/l.

Circular dichroism spectroscopy

CD spectra were obtained on an Aviv Model 62DS spectropolarimeter calibrated with an aqueous solution of ammonium *d*-(+)camphorsulfonate. The measurements were obtained on ZnXPA-MBD and CdXPA-MBD solutions in NMR buffer with, and without, 15% (v/v) glycerol at 25°C in a quartz cell of 0.1 cm path length. The samples were of approximately equal concentration estimated at 0.02 mM using the Bradford assay. Each spectrum was the result of averaging two consecutive scans from 250 to 195 nm recorded with a bandwidth of 1.0 nm and a time constant of 1.0 s. Following the subtraction of a blank spectrum of either water or 15% aqueous glycerol, the data were smoothed with a binomial function. Thermal denaturation curves for both proteins were obtained by recording CD spectra at 2.5°C intervals from 5 to 80°C, at 220 nm.

EXAFS spectroscopy

The EXAFS data were collected at the Stanford Synchrotron Radiation Laboratory (beamline 4.2) under dedicated operating conditions (3.0 GeV and 40–90 mA current). Five milligrams of CdXPA-MBD in NMR buffer was lyophilized, pressed into a holder (1.5×0.25 cm), sealed with Kapton tape, and frozen at ~77 K in a liquid nitrogen cryostat. Approximately 2 mM samples of ZnXPA-MBD and CdXPA-MBD in NMR buffer containing 15% glycerol were loaded into a specially designed 125 µl cell holder and frozen at ~77 K with liquid nitrogen. The beam size for all the experiments was 1.0×0.1 cm. Spectra for ZnXPA-MBD and CdXPA-MBD were collected at the zinc and cadmium K-edges, respectively, in the fluorescence mode, using an energy-resolving 13-element germanium detector. The spectrum of a ZnS standard was collected in transmission mode at 300 K. Energy calibration for the zinc K-edge EXAFS was made by assigning the first inflection point in the absorption edge of zinc foil to 9659 eV. Similarly, energy calibration for the cadmium K-edge EXAFS was made by assigning the first inflection point in the absorption edge of cadmium foil to 26 711 eV. The absorption spectra were normalized by fitting polynomials through the pre- and post-edge regions. At E_0, the value of the extrapolated pre-edge was set to 0 and the difference between the extrapolations of the pre- and post-edge polynomials was set to 1.

The EXAFS oscillations were extracted by fitting a polynomial spline function through the post-edge region and normalizing the difference between this approximation of the solitary-atom EXAFS and the actual data with the absorption decrease calculated using the McMaster tables (30). Fourier transforms were taken over photoelectron wavevector ranges that varied on the basis of the signal-to-noise ratio for each element. EXAFS nodes were selected as endpoints to the Fourier transform range and a 2σ-wide Gaussian window was used to dampen the EXAFS oscillations at the endpoints.

The phase and amplitude for the cation–sulfur path were calculated using the *ab initio* code FEFF7.02 (31). The normalized phase and amplitudes of the cation–sulfur scattering paths were used to fit the experimentally measured EXAFS. The ZnS and CdS T^2_d structures were used to approximate the metal cation tetrahedral environment in both proteins. The number of sulfur atoms was determined by using the normalized phase and amplitude to fit the ZnS standard EXAFS data which was multiplied by a scale factor of 0.9 to give a sulfur atom value of 3.9 atoms, a value in good agreement with the expected value of 4.0 atoms. Typically, scale factors between 0.8 and 1.0 are used to fit experimental EXAFS amplitudes with those calculated by FEFF7.02 (31). The same scale factor was applied to the fitting results for both ZnXPA-MBD and CdXPA-MBD.

NMR spectroscopy

NMR samples of ZnXPA-MBD and CdXPA-MBD (1.5 mM) were prepared in 600 µl of 90% H_2O/10% D_2O in the following NMR buffer: 20 mM K_2HPO_4, 100 mM KCl, 25 mM DTT_{d10}, 50 µM NaN_3, pH 7.3. Two-dimensional ^{1}H,^{15}N-heteronuclear single quantum coherence (HSQC) (32,33) and three-dimensional ^{15}N-edited HSQC (33) spectra were collected at 30°C on a Varian 750- or 500-Unityplus spectrometer.

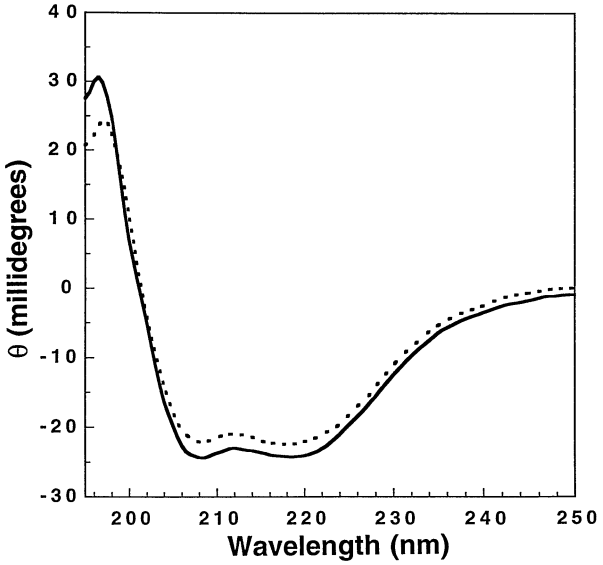

Fig. 1. Circular dichroism spectra for ZnXPA-MBD in NMR buffer (solid line) and in NMR buffer containing 15% glycerol (dashed line). Due to the uncertainty in the protein concentration determined by the Bradford assay, the spectra are displayed in units of millidegrees.

Table I. Helical parameters R_1 and R_2 for ZnXPA-MBD and CdXPA-MBD at 25°C, pH 7.2[a]

Sample	R_1	R_2
ZnXPA-MBD	–1.13	1.04
ZnXPA-MBD (15% glycerol)	–0.94	1.02
CdXPA-MBD	–1.05	0.93
CdXPA-MBD (15% glycerol)	–1.19	0.99

[a]Calculated as described by Rizo *et al*. (37). R_1 is the ratio between the intensity of the maximum between 190 and 195 nm and the intensity of the minimum between 200 and 210 nm. R_2 is the ratio between the intensity of the minimum near 222 nm and the intensity of the minimum between 200 and 210 nm.

Results

Circular dichroism spectroscopy

The CD spectrum for ZnXPA-MBD shown in Figure 1 (solid line) is characteristic of a protein with substantial secondary structure. The double minima near 222 and 208–210 nm plus the distinct maximum between 190–195 nm are characteristic of a peptide containing significant helical structure (34). Figure 1 shows the CD spectrum for ZnXPA-MBD (dashed line) after the addition of 15% (v/v) glycerol to the original sample. Except for a small decrease in intensity due to dilution, the CD profiles for ZnXPA-MBD are identical in both solutions, indicating that 15% aqueous glycerol does not affect the solution structure of ZnXPA-MBD. The CD profiles observed for CdXPA-MBD in the presence and absence of glycerol were similar to each other and similar to that observed for ZnXPA-MBD.

Because mean molar ellipticity values used to deconvolute CD spectra are sensitive to many factors (35), the CD data were analyzed using two parameters, R_1 and R_2, which are independent of inaccuracies in determining protein concentrations as well as those caused by small shifts in wavelength (36,37). For a random structure R_1 is positive and R_2 close to 0; in a highly helical structure R_1 is near –2 and R_2 approaches 1. Such parameters, tabulated in Table I, are similar for both

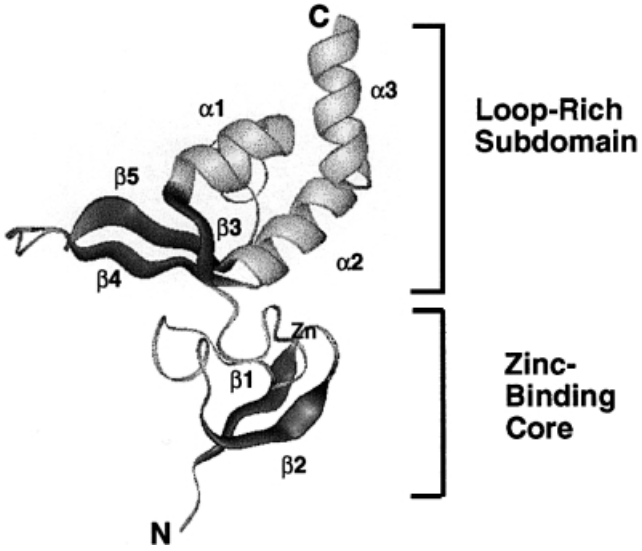

Fig. 2. Ribbon representation of the average structure for XPA-MBD as determined by NMR-based distance geometry methods (17). The secondary structural features are labeled. Residues D101–K137, zinc-binding core; residues L138–F219, loop-rich subdomain.

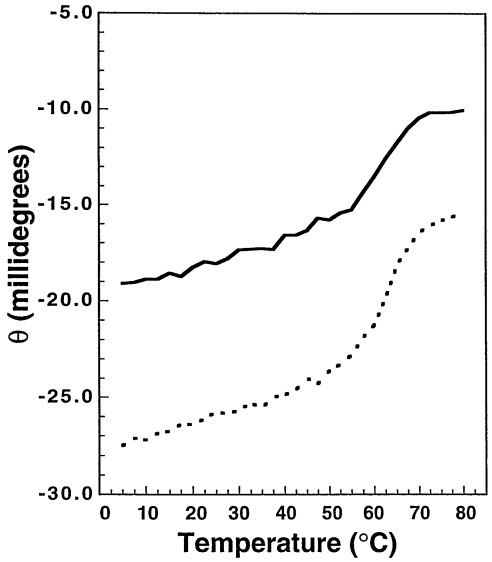

Fig. 3. Thermal melts for ZnXPA-MBD (solid line) and CdXPA-MBD (dashed line). The data were collected at 220 nm in 2.5°C intervals between 5 and 80°C. The difference in the absolute position of the temperature melts is caused by different protein concentrations.

ZnXPA-MBD and CdXPA-MBD in the presence or absence of 15% glycerol, suggesting that the solution structures of both proteins are similar in both solutions. While the R_1 and R_2 values indicate that ZnXPA-MBD and CdXPA-MBD are not randomly coiled in solution, the intermediate range of the R_1 and R_2 values indicates that the protein is not predominantly helical. This is corroborated by the NMR-derived solution structure for XPA-MBD illustrated in Figure 2 (17). The protein consists of two subdomains; a zinc-binding core composed of one anti-parallel β-sheet and one long 'turn', and a loop-rich subdomain composed of a triple-stranded antiparallel β-sheet, three α-helices, one short turn and three loops.

Figure 3 shows CD temperature melts for ZnXPA-MBD and CdXPA-MBD in NMR buffer. In general, the CD melts

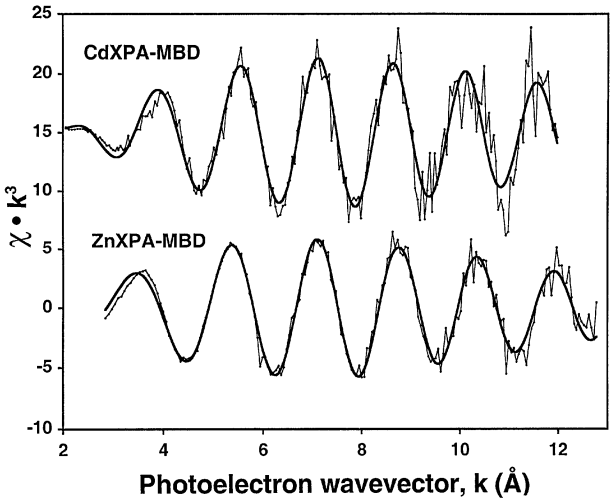

Fig. 4. EXAFS spectra for ZnXPA-MBD and CdXPA-MBD in 15% frozen aqueous glycerol solution at ~77 K. The paler line is a plot of experimental data and the darker line is the fit of the experimental data.

for both proteins are similar, suggesting little, if any, difference in the stability between the zinc- and cadmium-containing proteins. The uneven appearance of the melt below ~50°C, together with the rise of the slope in this range, is indicative of unraveling of individual units of secondary structure (38). As shown in Figure 2, XPA-MBD has a prolate global shape with α-helices located in the C-terminal subdomain (17). Helices are less stable than β-sheet and, therefore, the shape of the CD temperature melts below ~50°C probably results from the unraveling of α-helices in the loop-rich subdomain (38). Above ~50°C the melt is characteristic of a cooperative transition with an inflection point of ~62°C. After cooling the samples back to 25°C, the profiles of the CD spectra were similar to those of the original spectra except for an ~20% decrease in intensity (measured at 220 nm), suggesting that denaturation was not completely reversible.

EXAFS spectroscopy

Because the CD spectra indicated that the structures of ZnXPA-MBD and CdXPA-MBD were not affected by the presence of 15% aqueous glycerol in the aqueous solution, EXAFS data were collected for both proteins in this medium. Figure 4 compares the EXAFS for ZnXPA-MBD and CdXPA-MBD in frozen 15% aqueous glycerol (the paler lines). In addition to unambiguously identifying the element at the metal center, the analysis of the EXAFS oscillations provides information on interatomic distances, the number and type of ligand atoms and the statistical and/or thermal disorder of the shells of atoms around the metal center (39) and has been successfully used to characterize the local structural environment around metals in a variety of metalloproteins (29,40–43). The difference in phase between the ZnXPA-MBD and CdXPA-MBD EXAFS can be attributed to a combination of the difference in the absorber phase shift with Z and the abitrary assignment of the ionization threshold, E_0, which is the basis for calculating the wave vector magnitude from the energy. The EXAFS oscillations for ZnXPA-MBD and CdXPA-MBD were fitted over the magnitude of the photoelectron wavevector region of ~2–13 Å and the results for the frozen 15% glycerol samples are shown by the darker line in Figure 4. Both metalloproteins are well fitted by a single sulfur scattering wave. Table II contains the quantitative fitting results and shows that the

Table II. Fitting results to the EXAFS spectra for ZnXPA-MBD, CdXPA-MBD and ZnS in 15% frozen aqueous glycerol or lyophilized (L)[a]

Sample	Distance (Å)	Number	σ	r^2	dE_0
ZnXPA-MBD	2.34 ± 0.01	4.3 ± 1.1	0.00 ± 0.00	1.9477	–1.9 ± 3.1
ZnXPA-MBD (L)	2.34 ± 0.01	4.4 ± 0.9	0.03 ± 0.04	0.8114	–1.4 ± 3.1
CdXPA-MBD	2.53 ± 0.02	4.6 ± 1.2	0.06 ± 0.02	2.0328	0.5 ± 3.7
CdXPA-MBD (L)	2.54 ± 0.01	4.4 ± 1.0	0.03 ± 0.02	1.0505	2.7 ± 3.3
ZnS (L)	2.33 ± 0.02	3.9 ± 0.7	0.04 ± 0.02	0.8893	–2.7 ± 2.4

[a]The uncertainties were determined as the amount by which a parameter could be varied from the value giving the best fit as to increase r^2 by 10% from its minimum value. The data for ZnXPA-MBD (L) and ZnS (L) are from Hess *et al.* (29).

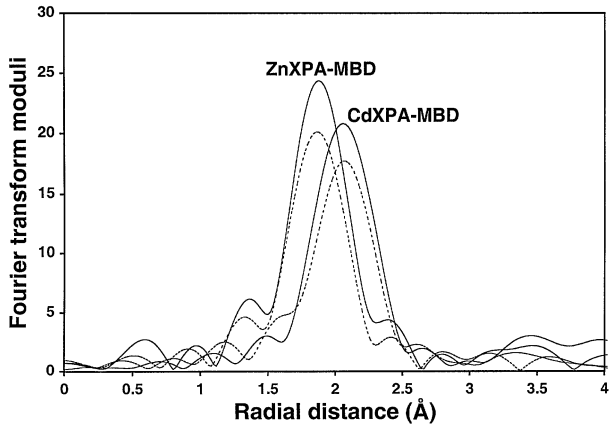

Fig. 5. Fourier transforms of the ZnXPA-MBD and CdXPA-MBD EXAFS profiles over the photoelectron wavevector region from ~2 to 13 Å. The solid line is for the sample in 15% frozen aqueous glycerol solution and the dashed line is for the lyophilized sample. The major peak in each of the Fourier transforms is due to sulfur atoms. The peaks in the Fourier transforms are not corrected for phase shifts and appear shorter than the actual distance from the absorber to the neighboring atoms.

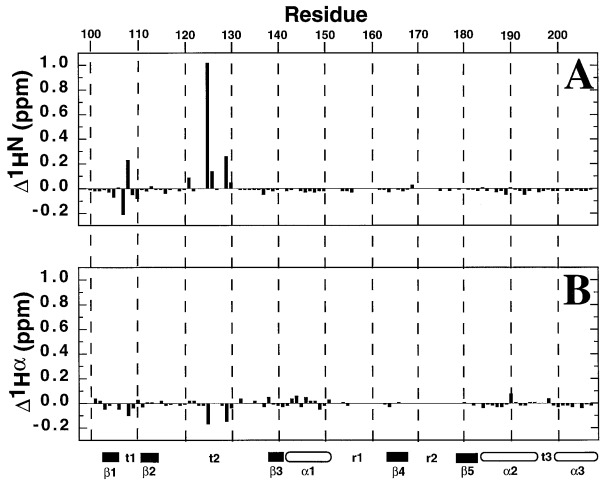

Fig. 6. The $^1H^N$ (**A**) and $^1H^\alpha$ (**B**) chemical shift differences between ZnXPA-MBD and CdXPA-MBD, defined as the chemical shift of ZnXPA-MBD minus the chemical shift of CdXPA-MBD.

metal in both proteins are coordinated by four sulfur atoms in the lyophilized and frozen 15% aqueous glycerol states.

Fourier transforms of the EXAFS oscillations for ZnXPA-MBD and CdXPA-MBD, lyophilized and in frozen 15% aqueous glycerol, are compared in Figure 5. Because the Fourier transforms are not corrected for phase shifts the peaks appear 0.2–0.5 Å shorter than the actual distance from the absorber to the neighboring atoms. In all four samples, the major peak observed in the Fourier transform of the EXAFS spectra results from the backscattering amplitude of sulfur atoms. The sulfur amplitude peak is in exactly the same position for both the lyophilized and frozen 15% aqueous glycerol XPA-MBD sample containing the same metal. The only difference between the lyophilized and frozen 15% glycerol sample is that the maximum intensity of the former sample is slightly lower, probably reflecting greater disorder in the lyophilized sample. The radial distance of the sulfur amplitude peak is greater for CdXPA-MBD than for ZnXPA-MBD, reflecting a longer metal–sulfur bond length in the cadmium-associated protein. The quantitative fitting results shown in Table II indicate that the zinc–sulfur bond is the same length in both the lyophilized and frozen 15% aqueous glycerol ZnXPA-MBD samples, at 2.34 Å. The cadmium–sulfur bond lengths for both the lyophilized and frozen 15% aqueous glycerol CdXPA-MBD samples are also essentially identical, 2.54 Å.

The 2.34 Å zinc–sulfur bond length determined for human ZnXPA-MBD is identical to the zinc–sulfur bond length determined at the metal center of full-length *Xenopus laevis* XPA (43). An identical zinc–sulfur bond length was also observed at the metal center of the *E.coli* UvrA protein, a damage recognition subunit of ABC excision nuclease that contains a C4-type zinc-binding motif (40). The 2.54 Å cadmium–sulfur bond length determined for CdXPA-MBD is identical to that determined for cadmium complexes with metallothioneins (44,45) and phytochelatins (46,47), cysteine-rich, heavy metal chelating proteins in animals and plants, respectively. As observed for UvrA, metallothioneins and phytochelatins, the EXAFS data for ZnXPA-MBD and CdXPA-MBD contain no evidence to indicate that the metal is coordinated to the imidazole nitrogen of a histidine residue. Proteins containing zinc-binding motifs tetrahedrally coordinated to one (C3H1) or two (C2H2) histidine residues are common (19). EXAFS spectra of cysteine–histidine, hetero-residue zinc-binding motifs are more complex because of the presence of a shorter (1.94 Å) zinc–nitrogen bond. Consequently, such EXAFS profiles display oscillations composed of multiple components and the corresponding Fourier transforms have additional peaks (41,42). The EXAFS data collected for ZnXPA-MBD and CdXPA-MBD do not display oscillations due to multiple components nor do the corresponding Fourier transforms of the EXAFS profiles contain additional peaks due to nitrogen, confirming that the metal in ZnXPA-MBD and CdXPA-MBD is coordinated only with sulfur atoms.

NMR spectroscopy

Figure 6A is a plot of the chemical shift changes of the $^1H^N$ resonances of XPA-MBD upon the substitution of Cd^{2+} for Zn^{2+}. The backbone nuclei, $^1H^N$ and ^{15}N, are sensitive to perturbations to the chemical environment brought about by

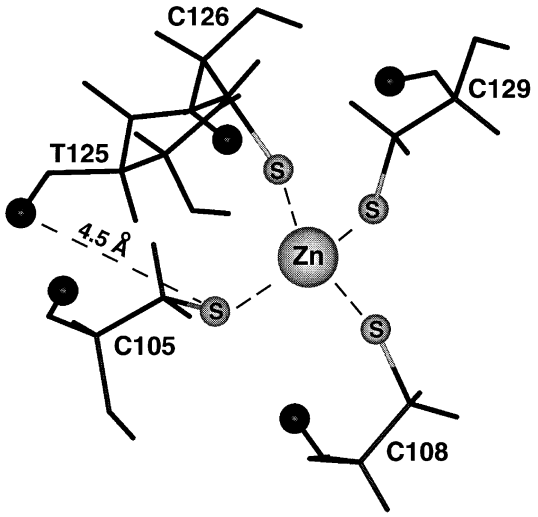

Fig. 7. The average orientation of C105, C108, T125, C126 and C129 about the Zn^{2+} in XPA-MBD from Figure 2 (17). The sulfur atoms are labeled 'S', the backbone amide protons are shown as black spheres and the metal–sulfur bonds are indicated by dashed lines. The distance from T125 $^1H^N$ to the nearest sulfur atom (C126, $^{32}S^{\gamma}$) is also illustrated.

physical or structural changes to the protein (16–18,48). By identifying the residues whose $^1H^N$–^{15}N HSQC cross peaks undergo a metal-dependent chemical shift perturbation it is possible to map the location of the structural changes on to the three-dimensional structure of the protein. Figure 6A illustrates that the substitution of Cd^{2+} for Zn^{2+} only effects changes in the $^1H^N$ resonances in the zinc-binding subdomain of XPA-MBD and that these changes are localized about the four cysteine residues that chelate the metal. The absence of significant $^1H^N$ resonance changes outside the immediate vicinity of the metal-binding site indicates that substitution of Cd^{2+} at the metal site does not alter the gross structure of XPA-MBD (49). This is corroborated in Figure 6B, a plot of the change in the chemical shift of the $^1H^{\alpha}$ resonances upon substituting Cd^{2+} for Zn^{2+} in XPA-MBD. The backbone $^1H^{\alpha}$ chemical shifts are sensitive to the protein's secondary structure (50) and only residues C105, T125 and C129 shift by $>$0.05 p.p.m. when the Zn^{2+} is replaced with Cd^{2+}. Further evidence that ZnXPA-MBD and CdXPA-MBD have essentially identical tertiary structures is obtained from the three-dimensional ^{15}N-edited NOESY spectrum for each protein. NOESY cross peaks are observed between protons that are within 5 Å of each other and the cross-peak patterns in the ^{15}N-edited NOESY experiment for ZnXPA-MBD and CdXPA-MBD are essentially identical (data not shown).

While the NMR data indicate that there are no major differences in the overall structure of ZnXPA-MBD and CdXPA-MBD, the data in Figure 6 suggest that something is occurring at the vicinity of the metal-binding site. From the EXAFS data it is known that the metal–sulfur bond in the Cd^{2+} form of XPA-MBD is ~0.2 Å longer than that in the Zn^{2+} form. This will affect any hydrogen bonds involving sulfur atoms coordinated to the cadmium because both the electron density at the sulfur and the hydrogen bond length will be different. Therefore, the chemical shift changes observed in Figure 6A all probably arise from changes in the hydrogen bonding network about the metal site (51). Figure 7 highlights the region around the metal site for the average refined structure of XPA-MBD (17). Ikegami *et al*. (18,52) reported six hydrogen bonds between the $^{32}S^{\gamma}$ of C105, C108 and C126 and the $^1H^N$ of C108, E107, K110, N128, C129 and C126. These restraints were introduced into the final stages of their structure refinements on the basis of slow exchange of the amide protons and structure calculations. Although we also observed slowly exchanging $^1H^N$ resonances for the four cysteine zinc-chelating residues and residues neighboring these amino acids (16), we did not introduce any hydrogen bonds into our structure refinements because, from our structure calculations, the possible hydrogen bonding pattern was ambiguous. Furthermore, the data in Figure 6A show that the $^1H^N$ chemical shifts of C108, C126 and C129 are the most perturbed cysteine residues upon substituting Cd^{2+} for Zn^{2+}, indirectly supporting only some of the hydrogen bonds reported by Ikegami *et al*. (18,52) around the metal site. Indeed, Figure 6B shows that the most perturbed amide is for T125, which becomes shielded by $>$1.0 p.p.m. with the substitution of Cd^{2+}. The amide of T125 slowly exchanges with H_2O (16) and the upfield direction of the chemical shift change upon substituting Zn^{2+} with Cd^{2+} suggests that a hydrogen bond has been broken. However, as illustrated in Figure 7, the nearest possible proton acceptor is the sulfur atom of C126 which is 4.5 Å away, a distance well beyond the typical ~2.0 Å hydrogen bond length (53). Consequently, while it is not possible to identify the hydrogen bond acceptor for $^1H^N$ of T125, the substitution of Cd^{2+} for Zn^{2+} in XPA-MBD disturbs the metal site such that a hydrogen bond involving the amide of T125 is probably broken.

Discussion

One possible mechanism for the mutagenicity of cadmium is that it displaces the zinc in XPA and that the resulting structural changes to XPA hinder, or prevent, the protein from binding damaged DNA or from interacting with other NER proteins (26,28). Such a hypothesis is based upon the greater affinity of Cd^{2+} over Zn^{2+} for sulfur ligands due to the hard–soft acid–base effect (54,55). The EXAFS data presented here indicate that the metal–sulfur bond in CdXPA-MBD is ~0.2 Å longer than that in ZnXPA-MBD. However, both the CD and NMR data show that such a difference in the metal–sulfur bond length does not result in any detectable structural changes to the protein. The only notable difference between the two proteins is in the hydrogen bond network about the metal site where the hydrogen bonding must apparently change in order to accommodate differences in the metal–sulfur bond length. Therefore, even if Cd^{2+} replaces Zn^{2+} at the metal-binding site in XPA, the mutagenic effects of cadmium are probably brought about by another mechanism(s). One possibility is that cadmium may bind to negatively charged surface residues on XPA; such binding, while not necessarily altering the structure of XPA, may interfere with DNA binding. Another possibility is that cadmium's mutagenicity results from its association with DNA rather than with NER proteins. Such a conclusion is supported by *in vitro* competition studies with human cell extracts, which showed that addition of Zn^{2+} to the cell extracts inhibited NER more than addition of Cd^{2+} (56). *In vitro* studies show that Cd^{2+} interferes with the fidelity of DNA synthesis (57) and both Cd^{2+} and Zn^{2+} can bind to DNA (58,59). Given the importance of counterions in stabilizing the structure of DNA at specific sites on the phosphodiester backbone (60), and the basic protrusion in the loop-rich subdomain of XPA which may bind DNA through non-specific contacts with the acidic phosphodiester DNA backbone (17),

the mutagenic properties of Cd^{2+} may be related to its association with DNA rather than XPA or other NER proteins (61). Efforts are in progress in our laboratory to investigate the role of metal binding to DNA and the effects these metals have on the binding of XPA to DNA.

Acknowledgements

We thank Drs Naxing Xu and Richard D.Smith for the mass spectral analyses, Dr Steven D.Conradson for the use of equipment essential for EXAFS data collection, Dr Nancy G.Isern for technical support, Dr Andrew S.Lipton for computer support, and Drs David F.Lowry, John R.Cort and Paul D.Ellis for discussions. The Stanford Synchrotron Radiation Laboratory is funded by Basic Energy Sciences, Department of Energy. This work was performed under the auspices of the US Department of Energy (contract DE-AC06-76RLO1830) and was supported by the Department of Energy Office of Biological and Environmental Research Program under grant 249311 KP11-01-01.

References

1. Cleaver,J.E. and Kraemer,K.H. (1989) Xeroderma pigmentosum and cockayne syndrome. In Scriver,S.C., Beaudet,A.L., Sly,W.S. and Valle,D. (eds) *The Metabolic Basis of Inherited Disease*. McGraw–Hill, New York, pp. 4393–4419.
2. Friedberg,E.C., Walker,G.C. and Siede,W. (1995) *DNA Repair and Mutagenesis*. American Society for Microbiology, Washington, DC, pp. 283–365.
3. Sancar,A. (1995) DNA excision repair. *J. Biol. Chem.*, **270**, 15915–15918.
4. Wood,R.D. (1997) Nucleotide excision repair in mammalian cells. *J. Biol. Chem.*, **272**, 23454–23468.
5. Mu,D., Hsu,D.S. and Sancar,A. (1996) Reaction mechanism of human DNA repair excision nuclease. *J. Biol. Chem.*, **271**, 8285–8294.
6. Cleaver,J.E. and States, J.C. (1997) The DNA damage-recognition problem in human and other eukaryotic cells: the XPA damage binding protein. *Biochem. J.*, **328**, 1–12.
7. Robins,P., Jones,C.J., Biggerstaff,M., Lindahl,T. and Wood,R.D. (1991) Complementation of DNA repair in xeroderma pigmentosum group A cell extracts by a protein with affinity for damaged DNA. *EMBO J.*, **10**, 3913–3921.
8. Jones,C.J. and Wood,R.D. (1993) Preferential binding of the xeroderma pigmentosum group A complementing protein to damaged DNA. *Biochemistry*, **32**, 12096–12104.
9. Asahina,H., Kuraoka,I., Shirakawa,M., Morita,E.H., Miura,N., Miyamoto,I., Ohtsuka,E., Okada,Y. and Tanaka,K. (1994) The XPA protein is a zinc metalloprotein with an ability to recognize various kinds of DNA damage. *Mutat. Res.*, **315**, 229–238.
10. Li,L., Elledge,S.J., Peterson,C.A., Bales,E.S. and Legerski,R.J. (1994) Specific association between the human DNA repair proteins XPA and ERCC1. *Proc. Natl Acad. Sci. USA*, **91**, 5012–5016.
11. Park,C.-H., Mu,D., Reardon,J.T. and Sancar,A. (1995) The general transcription-repair factor TFIIH is recruited to the excision repair complex by the XPA protein independent of the TFIIE transcription factor. *J. Biol. Chem.*, **270**, 4896–4901.
12. Matsuda,T., Saijo,M., Kuraoka,I., Kobayashi,R., Nakatsu,Y., Nagai,A., Enjoji,T., Masutani,C., Sugasawa,K., Hanoaka,F., Yasui,A. and Tanaka,K. (1995) DNA repair protein XPA binds replication protein A (RPA). *J. Biol. Chem.*, **270**, 4152–4157.
13. Wakasugi,M. and Sancar,A. (1999) Order of assembly of human DNA repair excision nuclease. *J. Biol. Chem.*, **274**, 18759–18768.
14. Sugasawa,K., Ng,J.M.Y., Masutani,C., Iwai,S., van der Spek,P.J., Eker,A.P.M., Hanaoka,F., Bootsma,D. and Hoeijmakers,J.H.J. (1998) Xeroderma pigmentosum group C protein complex is the initiator of global genome nucleotide excision repair. *Mol. Cell*, **2**, 223–232.
15. Kuraoka,I., Morita,E.H., Saijo,M., Matsuda,T., Morikawa,K., Shirakawa,M. and Tanaka,K. (1996) Identification of a damaged-DNA binding domain of the XPA protein. *Mutat. Res.*, **362**, 87–95.
16. Buchko,G.W., Ni,S., Thrall,B.D. and Kennedy,M.A. (1998) Structural features of the minimal DNA binding domain (M98–F219) of human nucleotide excision repair protein XPA. *Nucleic Acids Res.*, **26**, 2779–2788.
17. Buchko,G.W., Daughdrill,G.W., de Lorimier,R., Sudha,R.B.K., Isern,N.G., Lingbeck,J., Taylor,J-S., Wold,M.S., Gochin,M., Spicer,L.D., Lowry,D.F. and Kennedy,M.A. (1999) Interactions of human nucleotide excision repair protein XPA with DNA and RPA70ΔC327: chemical shift mapping and ^{15}N NMR relaxation studies. *Biochemistry*, **38**, 15116–15128.
18. Ikegami,T., Kuraoka,I., Saijo,M., Kodo,N., Kyogoku,Y., Morikawa,K., Tanaka,K. and Shirakawa,M. (1998) Solution structure of the DNA- and RPA-binding domain of human repair factor XPA. *Nature Struct. Biol.*, **5**, 701–706.
19. Berg,J.M. and Shi,Y. (1996) The galvanization of biology. A growing appreciation of the roles of zinc. *Science*, **271**, 1081–1086.
20. Miyamoto,I., Miura,N., Niwa,H., Miyazaki,J. and Tanaka,K. (1992) Mutational analysis of the structure and function of the xeroderma pigmentosum group A complementing protein. *J. Biol. Chem.*, **67**, 12182–12187.
21. Kennedy,M.A. and Ellis,P.D. (1989) ^{113}Cd nuclear magnetic resonance spectroscopy of Cd^{2+}-substituted heme and myoglobin. *J. Am. Chem. Soc.*, **111**, 3195–3203.
22. Zhang,F.L., Fu,H.-W., Casey,P.J. and Bishop,W.R. (1996) Substitution of cadmium for zinc in farnesyl:protein transferase alters its substrate specificity. *Biochemistry*, **35**, 8166–8171.
23. IARC (1993) *Beryllium, Cadmium, Mercury, and Exposures in the Glass Manufacturing Industry.* Monographs on the Evaluation of Carcinogenic Risks to Humans, Vol. 58. International Agency for Research on Cancer, Lyon.
24. Hartwig,A. and Beyersmann,D. (1989) Comutagenicity and inhibition of DNA repair by metal ions in mammalian cells. *Biol Trace Elem. Res.*, **21**, 359–365.
25. Nocentini,S. (1987) Inhibition of DNA replication and repair by cadmium in mammalian cells. Protective interaction of zinc. *Nucleic Acids Res.*, **15**, 4211–4225.
26. Hartmann,M. and Hartwig,A. (1998) Disturbance of DNA damage recognition after UV-irradiation by nickel (II) and cadmium (II) in mammalian cells. *Carcinogenesis*, **19**, 617–621.
27. Waalkes,M.P. and Misra,R.R. (1996) Cadmium carcinogenicity and genotoxicity. In Chang,L.W, Magos,L. and Suzuki,T. (eds) *Toxicology of Metals*. CRC Press, Boca Raton, FL, pp. 231–243.
28. Hartwig,A. (1995) Current aspects in metal genotoxicity. *Biometals*, **8**, 3–11.
29. Hess,N.J., Buchko,G.W., Conradson,S.D., Espinosa,F.J., Ni,S., Thrall,B.D. and Kennedy,M.A. (1998) Human nucleotide excision repair protein XPA: extended X-ray absorption fine-structure evidence for a metal-binding domain. *Protein Sci.*, **7**, 1970–1975.
30. McMaster,W.H., Kerr del Grande,N., Mallett,J.H. and Hubbell,J.H. (1969) *Compilation of X-ray Cross Sections.* University of California, Livermore, CA.
31. Rehr,J.J., Mustre de Leon,J., Zabinsky,S.I. and Albers.R.C. (1991) Theoretical X-ray absorption fine structure standards. *J. Am. Chem. Soc.*, **113**, 5135–5140.
32. Kay,L.E., Keifer,P. and Saarinen,T. (1992) Pure absorption gradient enhanced heteronuclear single quantum correlated spectroscopy with improved sensitivity. *J. Am. Chem. Soc.*, **114**, 10663–10665.
33. Zhang,O., Kay,L.E., Olivier,J.P. and Forman-Kay,J.D. (1994) Backbone ^{1}H and ^{15}N resonance assignments of the N-terminal SH_3 domain of drk in folded and unfolded states using enhanced-sensitivity pulsed field gradient NMR techniques. *J. Biol. NMR*, **4**, 845–858.
34. Holzwarth,G.M. and Doty,P. (1965) The ultraviolet circular dichroism of polypeptides. *J. Am. Chem. Soc.*, **87**, 218–228.
35. Hennessey,J.P. Jr and Johnson,W.C. Jr (1982) Experimental errors and their effect on analyzing circular dichroism spectra of proteins. *Anal. Biochem.*, **125**, 177–188.
36. Bruch,M.D., Dhingra,M.M. and Gierasch,L.M. (1991) Side chain backbone hydrogen bonding contributes to helix stability in peptides derived from an α-helical region of carboxypeptidase A. *Proteins: Struct. Funct. Genet.*, **10**, 130–139.
37. Rizo,J., Blanco,F.J., Kobe,B., Bruch,M.D. and Gierasch,L.M. (1993) Conformational behavior of *Escherichia coli* Omp A signal peptides in membrane mimetic environments. *Biochemistry*, **32**, 4881–4894.
38. Creigton,T.E. (1993) *Proteins: Structure and Molecular Properties*. W.H.Freeman, New York, pp. 287–291.
39. Teo,B.K. (1985) *EXAFS: Basic Principles and Data Analysis.* Springer-Verlag, Berlin.
40. Navaratnam,S., Myles,G.M., Strange,R.W. and Sancar,A. (1989) Evidence from extended X-ray absorption fine structure and site-specific mutagenesis for zinc fingers in uvrA protein of *Escherichia coli. J. Biol. Chem.*, **264**, 16067–16071.
41. Zhang,K. and Auld,D.S. (1995) Structure of binary and ternary complexes of zinc and cobalt carboxypeptidase A as determined by X-ray absorption fine structure. *Biochemistry*, **34**, 16306–16312.

42. Strange,R.W., Murphy,L.M., Karlsson,B.G., Reinhammar,B. and Hasnain,S.S. (1996) Effect of pH and ligand binding on the structure of the Cu site of the Met121Glu mutant of azurin from *Pseudomonas aeruginosa. Biochemistry*, **34**, 16391–16398.
43. Buchko,G.W., Iakoucheva,L.M., Kennedy,M.A., Ackerman,E.J. and Hess,N.J. (1999) Extended X-ray absorption fine structure evidence for a single metal binding domain in *Xenopus laevis* nucleotide excision repair protein XPA. *Biochem. Biophys. Res. Commun.*, **254**, 109–113.
44. Abrahams,I.L., Garner,C.D., Bremmer,I., Diakun,G.P. and Hasnain,S.S. (1985) Nature of the cadmium sites in rat liver metallothionein 1 from Cd K-edge EXAFS. *J. Am. Chem. Soc.*, **107**, 4596–4597.
45. Jiang,D.T., Heald.,S.M., Sham,T.K. and Stillman,M.J. (1994) Structures of the cadmium, mercury, and zinc thiolate clusters in metallothionein: XAFS study of Zn_7-MT, Cd_7-MT, Hg_7-MT, and Hg_{18}-MT formed from rabbit liver metallothionein 2. *J. Am. Chem. Soc*., **116**, 11004–11013.
46. Strasdeit,H., Duhme,A.-K., Kneer,R., Zenk,M.H., Hermes,Z. and Nolting,H.-F. (1991) Evidence for discrete $Cd(SCys)_4$ units in cadmium phytochelatin complexes from EXAFS spectroscopy. *J. Chem. Soc. Chem. Commun.*, **1991**, 1129–1130.
47. Pickering,I.J., Prince,R.C., George,G.N., Rauser,W.E., Wickramasinghe,W.A., Watson,A.A., Dameron,C.T., Dance,I.G., Fairlie,D.P. and Salt,D.E. (1999) X-ray absorption spectroscopy of cadmium phytochelatin and model systems. *Biochim. Biophys. Acta*, **1429**, 351–364.
48. Shuker,S.B., Hajduk,P.J., Meadows,R.P. and Fesik,S.W. (1996) Discovering high-affinity ligands for proteins: SAR by NMR. *Science*, **274**, 1531–1534.
49. Morita,E.H., Ohkubo,T., Kuraoko,I., Shirakawa,M., Tanaka,K. and Morikawa, K. (1996) Implications of the zinc-finger motif found in the DNA-binding domain of the human XPA protein. *Genes Cells*, **1**, 437–442.
50. Wishart,D.S., Sykes,B.D. and Richards,F.M. (1992) The chemical shift index: a fast and simple method for the assignment of protein secondary structure through NMR spectroscopy. *Biochemistry*, **31**, 1647–1651.
51. Goodfellow,B.J., Rusnak,F., Moura,I., Domke,T. and Moura,J.J.G. (1998) NMR determination of the global structure of the ^{113}Cd derivative of desulforedoxin: investigation of the hydrogen bonding pattern at the metal center. *Protein Sci.*, **7**, 928–937.
52. Ikegami,T., Kuroaka,I., Saijo,M., Kodo,N., Kyogoku,Y., Morikawa,K., Tanaka,K. and Shirakawa,M. (1999) Resonance assignments, solution structure, and backbone dynamics of the DNA- and RPA-binding domain of human repair factor XPA. *J. Biochem.*, **125**, 495–506.
53. Taylor,R. and Kennard,O. (1984) Hydrogen-bond geometry in organic crystals. *Acc. Chem. Res*., **17**, 320–326.
54. Pearson,G.K. (1966) Acids and bases. *Science*, **151**, 172–177.
55. Krizek,B.A., Merkle,D.L. and Berg,J.M. (1993) Ligand variation and metal ion binding specificity in zinc finger peptides. *Inorg. Chem*., **32**, 937–940.
56. Calsou,P., Frit,P., Bozzato,C. and Salles,B. (1996) Negative interference of metal (II) ions with nucleotide excision repair in human cell-free extracts. *Carcinogenesis*, **17**, 2779–2782.
57. Sirover,M.A. and Loeb,L.A. (1976) Infidelity of DNA synthesis *in vitro*: screening for potential metal mutagens and carcinogens. *Science*, **194**, 1434–1436.
58. Duane,M. (1974) Interactions of metal ions with nucleic acids. In Sigel,H. (ed.) *Metal Ions in Biological Systems.* Dekker, New York, pp. 1–43.
59. Waalkes,M.P. and Poirier,L.A. (1984) *In vitro* cadmium–DNA interactions: cooperativity of cadmium binding and competitive antagonism by calcium, magnesium, and zinc. *Toxicol. Appl. Pharmacol*., **75**, 539–546.
60. Saenger,W. (1983) *Principles of Nucleic Acids Structure.* Springer-Verlag, New York, NY, pp. 201–219.
61. Kasprzak,K.S. (1996) Oxidative DNA damage in metal-induced carcinogenesis. In Chang,L.W., Magos,L. and Suzuki,T. (eds) *Toxicology of Metals.* CRC Press, Boca Raton, FL, pp. 299–320.

Received November 3, 1999; revised December 28, 1999; accepted December 30, 1999